

Short wavelength effects on fast electron generation in fast ignition

H. Sakagami¹, R. Sato², A. Sunahara³, Y. Arikawa⁴, T. Johzaki⁵, H. Nagatomo⁴

¹*Fundamental Physics Simulation Div., National Institute for Fusion Science, Toki, Japan*

²*Department of Physics, Nagoya University, Nagoya, Japan*

³*Institute for Laser Technology, Osaka, Japan*

⁴*Institute of Laser Engineering, Osaka University, Osaka, Japan*

⁵*Mechanical Systems Engineering, Hiroshima University, Higashihiroshima, Japan*

1. Introduction

A fuel target is imploded by long-pulse implosion lasers and its compressed core is heated by a short-pulse ultrahigh-intense laser in the fast ignition scheme. FIREX experiments have started at ILE, Osaka University to demonstrate this scheme using Au cone-guided targets. But relatively small enhancement in neutron yield was achieved. Integrated simulations and basic experiments indicate that even the coupling efficiency from the heating laser to fast electrons is generally high but the divergence angle of fast electrons is large and their slope temperature is too high to deposit the energy into the core. Thus it results in lower coupling efficiency from fast electrons to the core [1].

As the slope temperature of fast electrons T_{fe} is scaled with $T_{fe} \propto (I_L \lambda_L^2)^{1/2}$ where I_L and λ_L are laser intensity and laser wavelength, respectively [2], using a shorter wavelength but same laser energy and focal spot size can reduce T_{fe} to heat the core more efficiently. Additionally, a number of fast electrons is increased when λ_L becomes short because the critical density of the laser, n_{cr} is also increased with the laser wavelength is becoming short as $n_{cr} \propto 1/\lambda_L^2$. Recently, a large-sized lithium borate (LiB_3O_5) crystal, which is used to convert fundamental laser beam into second harmonics to halve the wavelength, is available for high-power lasers on the market, and is planned to be installed into the LFEX laser rear-end system in near future.

Therefore characteristics of fast electrons, which are generated by the short wavelength laser, are investigated by 2D PIC simulations, and an enhancement effect for core heating due to the short wavelength is estimated.

2. Fast Electron Characteristics

As fast electrons are generated by the laser-plasma interaction inside the cone, they must penetrate the cone tip to reach the core. According to transport simulations, the fast electron

beam loses its power by 30% due to the collisional drag by the bulk electrons and the beam divergence becomes much larger due to the scattering by the highly ionized Au atoms during 10 μm propagation in the Au cone tip, and this leads to less efficient core heating [3]. To prevent this degradation, a low-Z material is preferable as the cone tip and we introduce Diamond-Like-Carbon (DLC) instead of Au as the cone material. On the other hand, as the fundamental wavelength of the heating laser LFEX is 1.05 μm , doubling (tripling) the frequency leads to 0.525 μm (0.35 μm) wavelength and we introduce these wavelengths in simulations.

First, preformed plasmas in front of the DLC cone tip are evaluated by STAR-1D [4] simulations using the Gaussian pre-pulse of 0.7 ns full width at half maximum and 10^{12} W/cm^2 peak intensity, because fast electron characteristics are much affected by the preformed plasma. Scale lengths of preformed plasmas are measured at 1 ns when the laser intensity reaches the peak value, and it is found that the scale length for each wavelength pre-pulse is almost proportional to the laser wavelength. As DLC is easily full ionized by the main pulse at an early stage, the maximum electron density should be same even for different wavelengths. We introduce the C^{6+} plasma with the preformed plasma that has the scale length of 2, 1 and 2/3 μm for 1.05, 0.525 and 0.35 μm wavelength lasers, respectively. As the density is normalized by the critical density for each wavelength and we assume $5n_{\text{cr}}$ as the maximum electron density for 0.35 μm , we should use $11.25n_{\text{cr}}$ for 0.525 μm and $45n_{\text{cr}}$ for 1.05 μm . But we introduce $10n_{\text{cr}}$ for 0.525 μm and $15n_{\text{cr}}$ for 1.05 μm due to limitation of computer resources. The plasma has 15 μm width and 10 μm thickness, and electron density profiles are shown in Fig. 1 for (a) 1.05, (b) 0.525 and (c) 0.35 μm wavelength lasers.

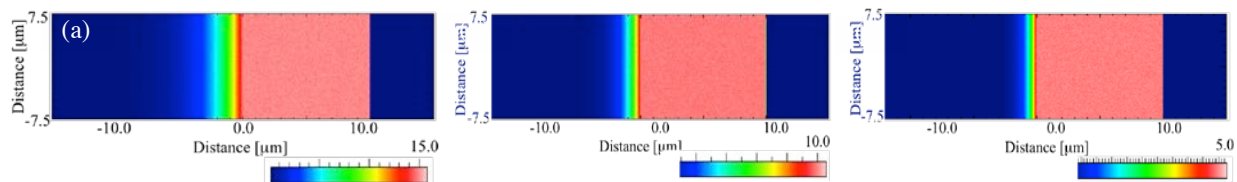


Fig. 1: Electron density profiles for (a) 1.05, (b) 0.525 and (c) 0.35 μm wavelength lasers.

The heating laser is set to $\lambda_{\text{L}}=1.05$, 0.525 or 0.35 μm , $I_{\text{L}}=10^{20}$ W/cm^2 , $\tau_{\text{rise}}=\tau_{\text{fall}}=25$ fs, $\tau_{\text{flat}}=500$ fs and plane wave or $\phi_{\text{FWHM}}=5$ μm Gaussian. Fast electrons are observed at 3.5 μm behind of the cone tip surface with 15 (± 7.5) μm width. To ignore a circulation of fast electrons, we introduce an artificial cooling region (2 μm width), in which fast electrons are gradually cooled down to the initial temperature, at 3.5 μm behind the observation region.

Electron energy spectra, which are time averaged by 50 fs after the fast electron beam

intensity reaches the steady state, are shown in Fig. 2 for (a) plane wave and (b) Gaussian wave. Reduction of the slope temperature and enhancement of the fast electron number due to the short wavelength are clearly seen, but the effects by the wavelength shortening in the case of Gaussian wave is smaller than that of plane wave, because Gaussian wave has a spatial profile in the transverse direction and only a center part of the beam has its peak intensity.

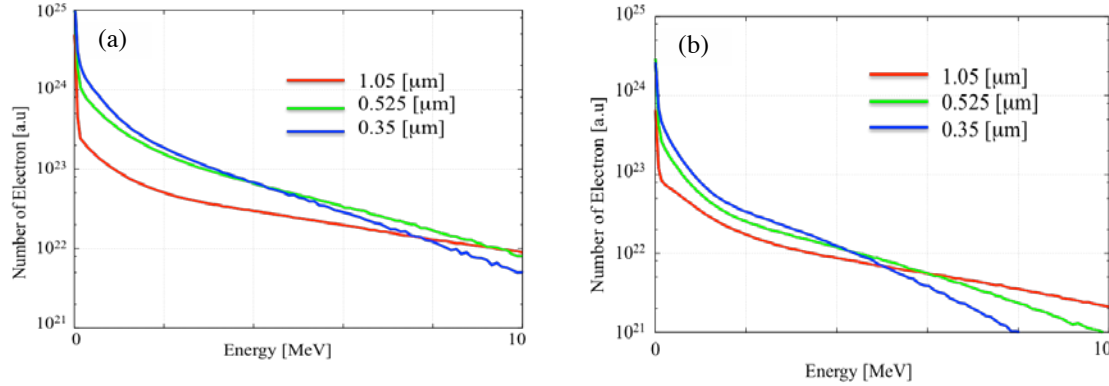


Fig. 2: Time averaged electron energy spectra for (a) plane wave and (b) Gaussian wave.

3. Short Wavelength Effects

We concentrate the energy range from 0.5 to 10 MeV and try to fit the energy spectrum with one slope temperature, namely $n(\varepsilon) = n_0 \exp(-\varepsilon/T_{fe})$, but we cannot fit it well due to an inflection point in the graph. Thus, we introduce to fit it with two slope temperatures, namely $n(\varepsilon) = n_L \exp(-\varepsilon/T_L) + n_H \exp(-\varepsilon/T_H)$, and results are summarized in Table 1 for the plane wave. The slope temperature of low energy region is scaled with $T_L \propto (I_L \lambda_L^2)^{1/3.05}$, so it does not follow 1/2 scaling, but 1/3 scaling [5]. We compare carrying energy by fast electrons with the energy range from 0.5 to 2 or from 2 to 10 MeV for different wavelengths, and results are also summarized in Table 1. As fast electrons with 0.5-2 MeV can deposit their energy into the core and efficiently heat the core, so efficiency of the core heating can be assumed to be proportional to carrying energy ratio of this energy range, and enhancement factor of 2.96 for 0.525 μm and 4.55 for 0.35 μm can be expected.

Table 1. Summary of two temperatures fitting for plane wave.

λ_L [μm]	n_L	T_L [MeV]	n_H	T_H [MeV]	Carrying energy ratio 0.5-2 [MeV]	Carrying energy ratio 2-10 [MeV]
1.05	1.58×10^{23}	0.83	5.04×10^{22}	5.88	1.00	1.00
0.525	8.01×10^{23}	0.63	2.13×10^{23}	3.23	2.96	1.88
0.35	2.43×10^{24}	0.39	3.76×10^{23}	2.44	4.55	1.93

Same evaluations for the Gaussian wave are summarized in Table. 2. The slope temperature of low energy region also follows 1/3 scaling, but the carrying energy ratio is

reduced comparing with the case of plane wave and 1.61 (2.26) times enhancement of the core heating can be expected for 0.525 (0.35) μm laser.

Table 2. Summary of two temperatures fitting for Gaussian wave.

$\lambda_L[\mu\text{m}]$	n_L	$T_L[\text{MeV}]$	n_H	$T_H[\text{MeV}]$	Carrying energy ratio 0.5-2[MeV]	Carrying energy ratio 2-10[MeV]
1.05	8.43×10^{22}	0.65	2.07×10^{22}	4.55	1.00	1.00
0.525	2.76×10^{23}	0.39	5.01×10^{23}	2.70	1.61	1.04
0.35	5.59×10^{23}	0.32	9.07×10^{22}	1.96	2.26	0.96

4. Wavelength Conversion

Recently, a lithium borate (LiB_3O_5) crystal block, which is large enough and applicable to high power laser, can be fabricated in China [6]. Four 10 x 10 cm size crystal plates, which are cut out from a large crystal block and polished, are placed onto a crystal holder, which is shown in Fig. 3 (a). The crystal holder will be introduced into the LFEX target chamber, which is shown in Fig. 3 (b), and we are going to test the halving wavelength conversion.

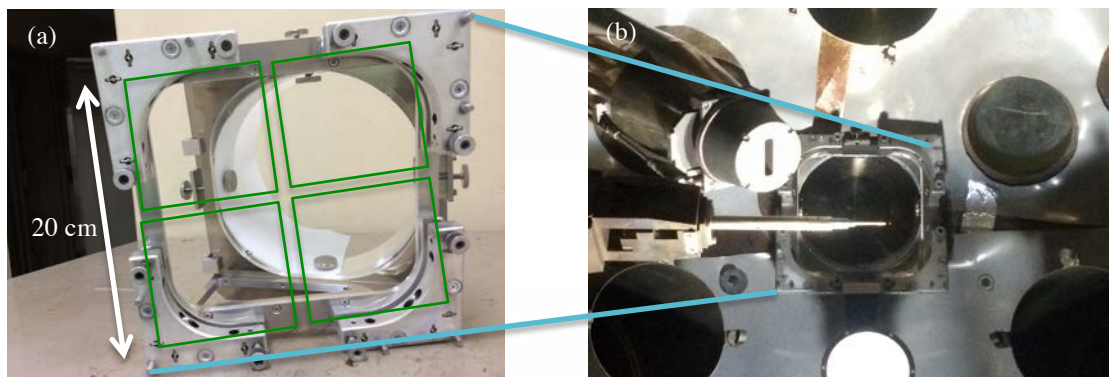


Fig. 3: Photographs for (a) crystal holder where 4 crystal plates are placed and (b) inside of target chamber.

Acknowledgments

This work is partially supported by JSPS KAKENHI Grant-in-Aid for Scientific Research (C)(16K05638) and (S)(15H05751), and is performed with the support and under the auspices of the NIFS Collaboration Research program (NIFS15KUGK093) and (NIFS12KUGK057).

References

- [1] T. Johzaki, et al., Nucl. Fusion **51**, 073022 (2011).
- [2] S. C. Wilks, et al., Phys. Rev. Lett. **69**, 1383 (1992).
- [3] T. Johzaki, et al., Phys. Plasma **16**, 062706 (2009).
- [4] A. Sunahara, et al., Plasma Fusion Res. **3**, 043 (2008).
- [5] F. N. Beg, et al., Phys. Plasmas **4**, 447 (1997).
- [6] H. Zhanggui, et al., J. Crystal Growth **335**, 133 (2011).